Magnetic and transport properties of Fe - Zr - B - (Cu) amorphous alloys

1997 J. Phys.: Condens. Matter 9 5671

(http://iopscience.iop.org/0953-8984/9/26/014)

J. Phys.: Condens. Matter **9** (1997) 5671–5685. Printed in the UK PII: S0953-8984(97)81257-X

Magnetic and transport properties of Fe–Zr–B–(Cu) amorphous alloys

J M Barandiarán†, P Gorria†‖, I Orúe†‖, M L Fernández-Gubieda†, F Plazaola†, J C Gómez Sal‡, L Fernández Barquín‡ and L Fournes§

† Departamento Electricidad y Electrónica, Universidad del Pais Vasco, PO Box 644, E-48080 Bilbao, Spain

‡ Física de la Materia Condensada, Universidad de Cantabria, E-39005 Santander, Spain

§ Laboratoire de Chimie du Solide, Université Bordeaux I, France

Received 24 January 1997

Abstract. FeZrB metallic glasses present magnetic properties that are enhanced compared to the pure FeZr ones. In particular, a large increase of the Curie temperature has been found. Magnetic and Mössbauer measurements show a decrease of the spin-glass character and a parallel homogenization of the hyperfine-field distribution as the boron concentration increases. Resistivity versus temperature measurements show a change in behaviour with B content: in the samples with small amounts of boron, a minimum in the resistivity versus temperature curves appears near the Curie temperature, while samples with high boron content show a low-temperature minimum, characteristic of most metallic glasses. The analysis of the results suggests that the evolution of the magnetic behaviour is related to changes in the density of states at the Fermi level, rather than to changes in the Fe–Fe distances. This is in agreement with published data on the specific heat of FeZr and FeB glasses. The influence of boron is shown to greatly enhance the weak itinerant ferromagnetism of FeZr glasses, leading to stronger ferromagnetic behaviour. The characteristic features of the resistivity are analysed in terms of localization effects on the conduction electrons, which extend to higher temperatures in the low-boron-content alloys.

1. Introduction

Fe-rich FeZr glasses have attracted much interest in the past few years [1–5]. They are among the most peculiar of the magnetic systems, displaying re-entrant spin-glass (RSG) behaviour and Invar characteristics. An initial theoretical explanation was based on the existence of magnetic inhomogeneities caused by variations of the Fe interatomic distances. This would lead to a non-collinear state with a net ferromagnetic component, developing a transverse spin freezing (TSF) when entering into the RSG state [6]. An alternative view has been proposed, which considers the existence of 'spin clusters' created by density variations during the casting of the ribbons [7]. In addition, it has been suggested that, even in these Fe-rich alloys, the observed magnetic phenomena are reminiscent of a superparamagnetic behaviour, with particular relaxation effects [8–10]. From an experimental point of view some facts are clearly established: the Curie temperature T_C increases with Zr content (up to about 25 at.% Zr, for which $T_C \approx 268$ K [11]), but the spin-glass temperature (T_{RSG}) decreases, vanishing at about 11 at.% Zr. On the other hand, the Curie temperature shows

‖ Present address: Departamento de Física, Universidad de Oviedo, Avenida Calvo Sotelo, s/n, E-33007 Oviedo, Spain.

0953-8984/97/265671+15$19.50

a large negative dependence on hydrostatic pressure, P (about -60 K GPa^{-1}) [4, 11]. This $T_C(P)$ dependence is greater in alloys with low Zr content (around 7 at.% Zr), which corresponds to the samples showing clearer spin-glass behaviour.

To achieve an understanding of the above-mentioned properties, it is useful to study the inclusion of atoms which could progressively distort the original atomic arrangement. Alloying with boron has been a common procedure for this purpose. In particular, FeZrB and FeZrBCu alloys have been extensively studied in the nanocrystalline state [12, 13], but so far little effort has been directed toward the pure amorphous phase of such alloys. A preliminary study on FeZrB glasses [14] shows that the effect of boron is to increase the Curie temperature of the alloys, which reaches room temperature. The iron magnetic moment also increases with boron content, but the general evolution of the spontaneous magnetization with temperature remains almost unchanged. This may indicate that the same exchange mechanisms should be present for FeZr and FeZrB glasses. On the basis of the Curie temperature dependence on pressure [15], and EXAFS experiments [16], it has been suggested that the effect of boron in FeZr cannot be related to changes in Fe–Fe distances, as they remain unchanged. This is probably due to an electronic transfer from B to the 3d band of Fe, which is larger than that from the Zr one. Such a transfer should alter the density of states at the Fermi level.

The thermal variation of the electrical resistivity in FeZr alloys has also been studied [17–20]. The absolute resistivity values lie in the range 150–160 $\mu\Omega$ cm. These alloys display interesting features, such as negative temperature coefficients and high-temperature (around 200 K) minima in the resistivity. The introduction of boron atoms can affect the transport properties, by modifying either the magnetic (electron–magnon scattering, and a RSG inhomogeneous state) or structural contributions, namely phonon and/or quantum electronic scattering.

The main aim of the present work is to improve our understanding of these effects in FeZrB(Cu) metallic glasses, through a systematic study of several magnetic quantities. We have performed DC and AC magnetometry, Mössbauer spectroscopy, and electrical resistivity (ρ-) measurements on a series of FeZrB glasses, whose compositions range from $Fe_{91}Zr_7B_2$ to $Fe_{80}Zr_{10}B_{10}$. Also, measurements were made on two samples without boron, $Fe_{91}Zr_9$ and $Fe_{90}Zr_{10}$, and another series with low Zr content, $Fe_{98-x}B_xZr_2$ ($x = 16$, 23 and 25), have been used to compare the results.

The compositional range includes alloys exhibiting spin-glass behaviour at low temperatures, and others with normal ferromagnetic behaviour. Therefore, the study of this large composition range can give some understanding of the magnetism of such alloys, as well as the features of Fe-rich amorphous alloys.

2. Experimental procedure

FeZrB(Cu) amorphous ribbons have been obtained by the melt-spinning (50 m s^{-1} linear speed) method under a controlled Ar atmosphere. Previously, stoichiometric quantities of the Fe (99.98%), Zr (99.8%), Cu (99.98%), and B (99.8%) elements were melted in an arc furnace. The labels and compositions (checked by electron microprobe analysis) of the samples are presented in table 1. The typical dimensions of their cross sections were 2 mm width and 20 μm thickness. They were shown to be amorphous by x-ray diffraction and Mössbauer spectroscopy. The Curie temperature and other magnetic properties (the evolution of the magnetization with temperature, in zero-field cooling (ZFC) or field cooling (FC); M versus $\mu_0 H$ isotherms up to 7 T; and hysteresis loops up to 0.3 T) were determined by means of a commercial SQUID magnetometer. Also, the magnetic AC susceptibility has

Table 1. Values for the Curie temperature, magnetic moment per Fe atom, β-exponent (used in the modified Arrott plots), a-parameter from equation (1) (see the text), room temperature resistivity, and temperature minima of the resistivity in the samples studied. The values in brackets show the estimated errors in the least significant figure.

Sample	Composition	T_C (K)	μ_{Fe} (μ_B)	β	a	$\rho_{295\,\mathrm{K}}$ ($\mu\Omega$ cm)	T_{min} (K)
B0/9	$Fe_{91}Zr_9$	220(5)	1.53(3)	0.323	4.4	122(3)	220(5)
B0/10	$Fe_{90}Zr_{10}$	230(5)	1.55(3)	0.372	2.7	—	250(5)
B2	$Fe_{91}Zr_7B_2$	230(5)	1.42(3)	0.325	4.8	122(3)	210(5)
B4	$Fe_{88}Zr_8B_4$	275(5)	1.66(3)	0.386	1.8	128(3)	290(5)
B6	$Fe_{87}Zr_6B_6Cu_1$	295(5)	1.63(3)	0.4	1.1	127(3)	300(5)
B10	$Fe_{80}Zr_{10}B_{10}$	365(5)	1.69(3)	0.48	0.3	138(3)	>330
B16	$Fe_{82}Zr_2B_{16}$	560(5)	2.01(4)	—	—	134(3)	≈30
B23	$Fe_{75}Zr_2B_{23}$	665(5)	2.04(4)	—	—	130(3)	≈30
B25	$Fe_{73}Zr_2B_{25}$	685(5)	2.05(4)	—	—	126(3)	≈30

been measured at a frequency of 85 Hz and 0.6 mT amplitude, between 4 and 300 K, in an induction magnetometer.

^{57}Fe Mössbauer transmission spectra of the samples B2, B4, and B6 have been recorded at liquid helium temperature in a conventional constant-acceleration spectrometer using a ^{57}Co–Rh source.

The electrical resistivity has been measured in the temperature range 4–300 K, by a four-point probe method using a low-frequency (80 Hz) AC current. Contacts were secured by spring-loaded tips, avoiding any kind of welding and surface crystallization.

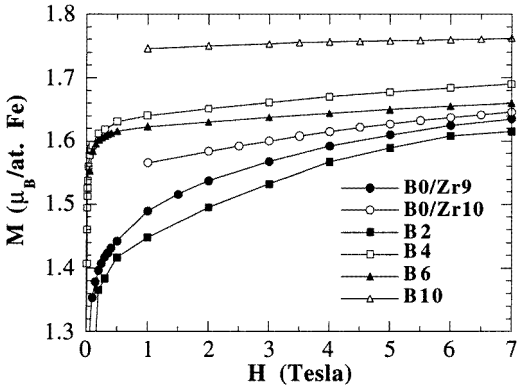

Figure 1. Magnetization curves up to 7 T for the samples B0, B2, B4, B6, and B10, obtained at 5 K.

3. Results

3.1. Magnetic measurements

3.1.1. The Curie temperature and magnetic moment. The magnetic parameters of the samples are summarized in table 1. The values of the Curie temperature, T_C, and magnetic moment per Fe atom, μ_{Fe}, of the FeZr alloys are difficult to obtain due to the large effect of the applied magnetic field. We have obtained the T_C-values from near-zero-applied-field

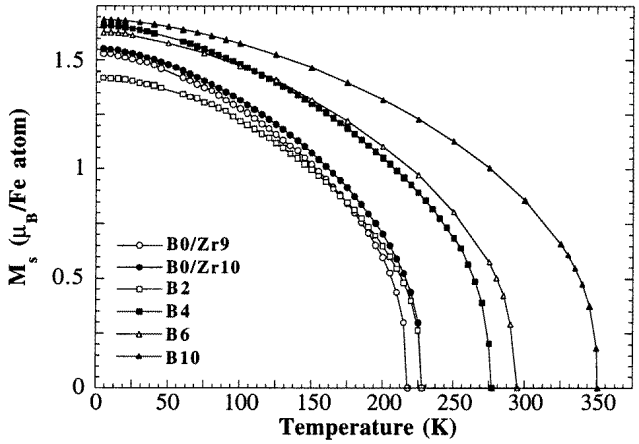

Figure 2. Thermomagnetization curves obtained from modified Arrott plots.

DC and AC measurements ($H_{app} < 40$ A m^{-1}). The two sets of measurements give the same values for T_C for all of the samples, and are in agreement with data from Mössbauer spectroscopy (see section 3.2). Figure 1 shows the magnetization at 5 K, and figure 2 shows the temperature dependence of the spontaneous magnetization, $M_s(T)$ (in Bohr magnetons per Fe atom), for samples with boron content $B = 0$, 2, 4, 6, and 10 at.%. The $M_s(T)$ curves have been obtained from modified Arrott plots, $M^{1/\beta}$ versus $(H/M)^{1/\gamma}$, given by the equation

$$M^{1/\beta} = a\left(\frac{H}{M}\right)^{1/\gamma} + M_s^{1/\beta}. \tag{1}$$

The values for the β- and γ-exponents were carefully chosen so that the isotherm at $T = T_C$ intersected at zero. The best value of the γ-exponent was 1.38, but the β-exponent varies from 0.32 for the $Fe_{91}Zr_9$ sample to 0.48 for the $Fe_{80}Zr_{10}B_{10}$ sample (see table 1). This procedure, used for all of the samples, ensures reliable values for μ_{Fe}, which can be compared from one sample to another. Furthermore, the β-values give a measurement of the inhomogeneity of the magnetism in the samples [21, 22], which increases as β departs from the value of 0.5. This indicates a higher inhomogeneity in low-boron-content samples. The values of the parameter a—see equation (1)—taken from the fittings at 0 K, can be associated with the forced paramagnetic susceptibility, χ_0, of the samples in the itinerant-magnetism framework [23]. The a-parameter decreases with the increase in boron content of the sample.

The magnetic moment has been calculated from the same modified Arrott plots at 1.8 K for all of the samples, and is reported in table 1. The magnetic moment of the FeZrB samples increases from 1.4 to 1.7 μ_B, with the increase of the boron content, reaching saturation. This also occurs in FeZr alloys for atomic contents of Zr above 10–11% [3].

For the B-rich (>15%) FeZrB samples we have observed an evolution of T_C similar to that for the FeB alloys [24]. The effect of Zr in these samples is to decrease the value of T_C by 70 K with respect to that for the same composition without Zr. The value of the μ_{Fe} for these samples is about 2 μ_B per Fe atom at 0 K, which is nearly the same as the values given by other authors for FeB alloys [25].

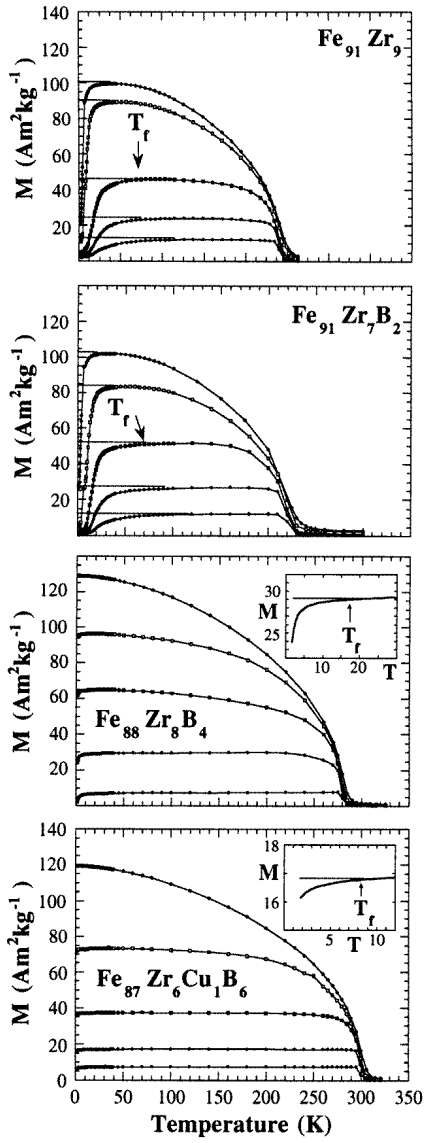

Figure 3. ZFC and FC $M(T)$ curves for the samples B0/Zr9, B2, B4, and B6 obtained at different applied magnetic fields (full circles, empty circles, full squares, empty squares, and full triangles correspond to $H_{app} =$ 0.4, 0.8, 1.6, 3.2, and 8 kA m^{-1} respectively). The insets in the plots corresponding to samples B4 and B6 show the differences between the ZFC and FC curves obtained at $H_{app} = 0.8$ kA m^{-1}.

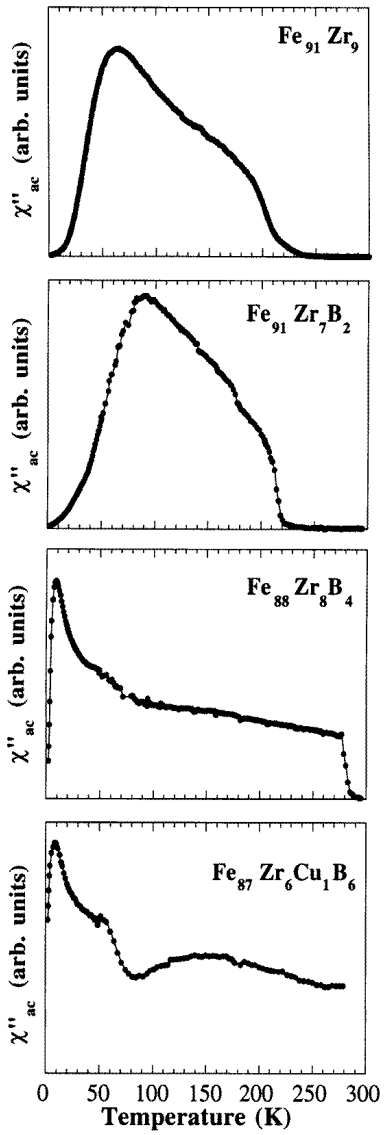

Figure 4. The evolution of the imaginary AC susceptibility χ'' versus the temperature for the samples B0/Zr9, B2, B4, and B6, measured at a frequency of 85 Hz, and 0.6 mT amplitude.

3.1.2. Low-temperature anomalous magnetic behaviour. Figure 3 shows the thermomagnetic curves for samples B0, B2, B4, and B6 measured at different applied magnetic fields (from 0.4 to 8 kA m^{-1}) for ZFC and FC. The ZFC is performed from 350 K to 1.8 K.

Samples are then heated to measure $M(T)$ up to $T > T_C$, after which they are re-cooled in the field used for the previous measurement (FC) to measure $M(T)$ again. The bifurcation of the heating and cooling curves at a certain 'freezing' temperature, T_f, is observed for the sample B0 and the sample B2. The value of T_f for these two compositions decreases when increasing the applied magnetic field up to 15 kA m^{-1}. For higher applied fields, no differences were observed between the two thermomagnetic curves. In the sample B4, the bifurcation occurs at lower temperatures, $T_f < 20$ K, and it is not observed for $H_{app} > 5$ kA m^{-1}. In the case of the sample B6, the ZFC and FC curves coincide for $T > 10$ K, and there is a slight difference, no larger than 1%, between the magnetization values at 1.8 K of the two curves. So the splitting occurs at a freezing temperature T_f lower than 10 K. For the sample B10, the differences between the ZFC and FC curves are negligible. This anomalous behaviour at low temperatures is usually related to a re-entrant spin-glass behaviour [1, 2, 4].

The results of the AC susceptibility measurements for samples B2, B4, and B6 are shown in figure 4. The real component (χ') coincides, in general, with the $M(T)$ results described above. The 'freezing' temperature T_f can be detected in χ'' (the imaginary out-of-phase susceptibility component) as a maximum at a temperature that coincides with the value of T_f obtained from thermomagnetic measurements. The approximate values for these maxima are 65 K (B0), 90 K (B2), 8 K (B4), and 4–5 K (B6). The Curie point is also clearly observed above 200 K.

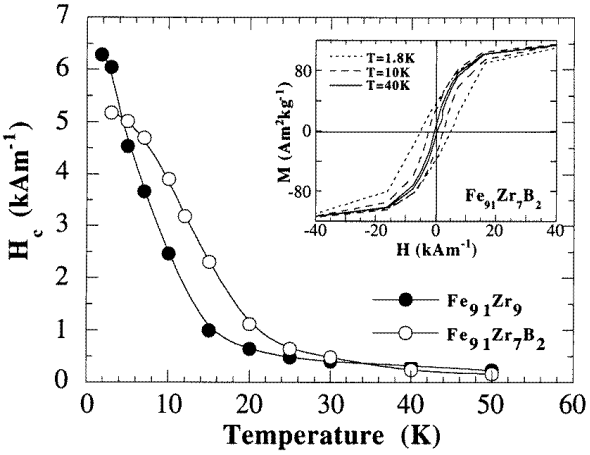

Figure 5. The temperature evolution of the coercive force for the samples B0/Zr9 and B2. The inset shows the hysteresis loops obtained at 1.8 K, 10 K, and 40 K.

Magnetic hysteresis loops have been measured by means of a SQUID magnetometer at various temperatures to obtain the evolution of the coercive force with temperature. In the case of samples B4 and B6, the coercive force, measured at 1.8 K, is below the experimental accuracy ($\approx$80 A m^{-1}), so no further measurements have been performed at higher temperatures. However, for the samples B0 and B2, the value of H_c at 1.8 K is around 5–7 kA m^{-1}, and this value decreases when the temperature increases, as observed in figure 5. The value of H_c strongly decreases to $\approx$0.8 kA m^{-1}, between 1.8 and 20 K. Increasing the temperature causes the coercive field to decrease to 0.15–0.2 kA m^{-1} at 50 K, and it remains almost constant at higher temperatures.

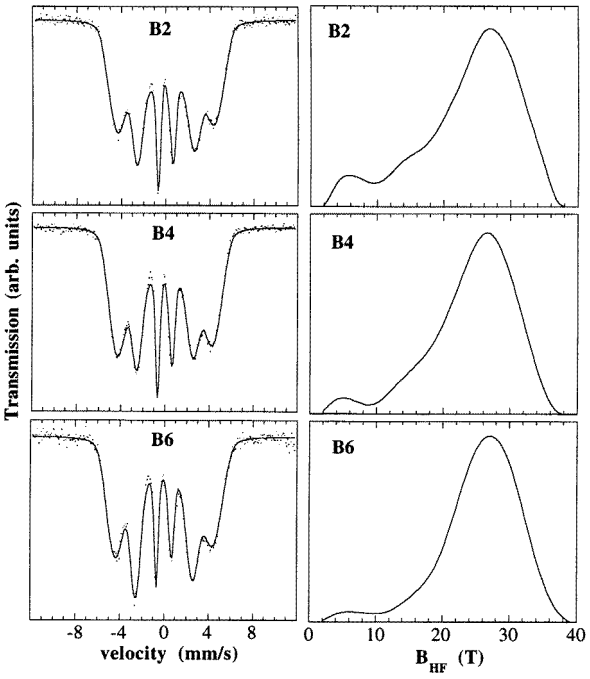

Figure 6. Mössbauer spectra (a) and hyperfine-field distributions (b) for the samples B2, B4, and B6 measured at 4 K.

3.2. Mössbauer measurements

All of the spectra, measured at $T = 4.2$ K, show the broad six-line pattern characteristic of a ferromagnetic amorphous alloy well below its Curie temperature (see figure 6). A prominent feature of these spectra is the increasing width from the inner to the outer lines, which is related to the existence of a distribution of local hyperfine fields. However, the pattern of the spectra further reveals the existence of two other line asymmetries. Firstly, labelling the lines from negative to positive velocities, the corresponding intensities follow the pattern $\Gamma_1 < \Gamma_6$, $\Gamma_2 > \Gamma_5$, and $\Gamma_3 > \Gamma_4$. This asymmetry is usually assigned to the correlation between the magnetic dipolar contribution and the electric field gradient [26], and appears in many other amorphous alloys. Secondly, one can observe that the positive-velocity lines are wider than the negative-velocity ones, which can be explained by assuming a linear correlation between the local hyperfine field, B_{HF}, and the local isomer shift, δ:

$$\delta(B_j) = \delta(B_0) + \alpha(B_j - B_0) \tag{2}$$

where B_0 is the lowest value for the hyperfine-field distribution, $P(B_{HF})$, and j runs over the allowed range of $P(B_{HF})$. The experimental data fittings were performed with the NORMOS program developed by Brand *et al* [27] for amorphous alloys, following the theoretical model of Billard and Chamberod [28], and Hesse *et al* [29], applied to the study of disordered Fe–Ni alloys. The electric field gradient (which is the origin of the quadrupolar perturbation) is considered to be randomly oriented with respect to the direction of the local hyperfine field, and so effectively averages to zero.

Table 2. Hyperfine parameters obtained from the Mössbauer spectra measured at 4 K for the samples B2, B4, and B6. $\hat{B}_{HF}$ is the average hyperfine field, and $\Delta\sigma$ is the half-width of the hyperfine-field distribution. The values of the isomer shift (IS) are with reference to that of a bcc-Fe foil measured at RT. Finally, D23 is the ratio of the second to the third Mössbauer peak, related to the magnetization distribution in the sample, and the parameter α is the same as that of equation (2).

	$\hat{B}_{HF}$ (T)	$\Delta\sigma$ (T)	IS (mm s^{-1})	D23	α (T mm^{-1} s)
B2	23.6(6)	7.4(1)	0.067(5)	1.75(3)	9.4×10^{-3}
B4	24.2(1)	6.5(1)	0.063(5)	1.56(4)	9.3×10^{-3}
B6	25.4(2)	6.2(2)	0.072(5)	2.14(3)	9.2×10^{-3}

The distributions of hyperfine fields, $P(B_{HF})$, shown on the right-hand side of figure 6, have been obtained by a smooth-histogram procedure in the same range of B_{HF} (0–40 T) for the three samples, B2, B4 and B6. The slope of the assumed linear relation between B_{HF} and δ takes the same value in the three cases; see table 2. The intensity ratio of the lines 1 and 3, D13, is kept fixed and equal to 3, while the corresponding ratio of the lines 2 and 3, D23, is allowed to vary; the resulting values are displayed in table 2. The most striking feature deduced from figure 6 concerns the shape of $P(B_{HF})$, which shows a low-field tail. This was also reported by Vincze *et al* [30] for FeZr alloys. As the boron content increases, the width of $P(B_{HF})$ decreases, and the tail at low fields, characteristic of B2, tends to disappear. The low-field tail is completely absent for the sample B16 [31], which is similar to the well known FeB amorphous alloys, showing a fully symmetric $P(B_{HF})$ distribution [24]. Together with the reduction of the $P(B_{HF})$ width, the increase of the B concentration causes the average hyperfine field to increase, giving an overall change of about 2 T from B2 to B6. This behaviour coincides with the increase of the magnetic moment per Fe atom. The D23 values are very similar for all of the samples, which indicates an almost random distribution of the magnetic moments in the samples.

Some Mössbauer spectra were measured at temperatures near T_C for the samples B2, B4, and B6, in order to confirm the values obtained from the magnetic measurements. For all of the samples, the temperature at which the distribution of B_{HF} disappears coincides with the value of T_C previously given, therefore confirming the Curie temperature values previously obtained.

3.3. Resistivity measurements

The electrical resistivity has been measured for all of the ribbons studied, between 4.2 K and 300 K. Some characteristic $\rho(T)$ curves are displayed in figure 7. In the Zr-rich samples (B0, B2, B4, B6, and B10), the resistivity decreases with increasing temperature, passing through a broad minimum at a temperature (T_{min}) which is always higher than 200 K. The values of these minima are given in table 1. Although the values of T_{min} do not coincide exactly with the T_C-values obtained from the magnetic measurements (see table 1), they increase roughly with the increasing boron content, as do the magnetic interactions. However, no changes in the $\rho(T)$ slope have been detected at the Curie temperature. This means that the magnetic contribution to the resistivity is very small compared with other effects such as residual, structural, and quantum contributions. It is important to note that the minimum appears for all of the Zr-rich samples, even those that do not exhibit low-temperature re-entrant spin-glass-like behaviour.

In the samples with a high boron content (B16, B23, B25), the resistivity versus

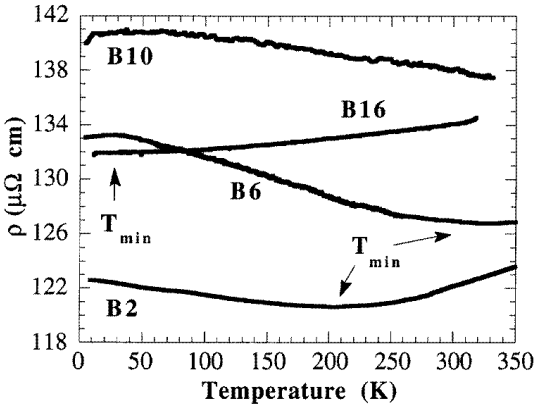

Figure 7. The resistivity versus the temperature evolution of the samples B2, B6, B10, and B16; the temperature minima are marked with arrows.

temperature shows a positive slope. A slight minimum appears at about 30 K, as for the FeB [32, 33] samples. It is worth mentioning that these minima, at low temperature, appear in many other B-containing metallic glasses [34, 35]. In particular, CoBSi samples show a minimum which shifts to higher temperatures with the increasing Si content. This behaviour was related to a decrease of the magnetic scattering [36].

The effect of a magnetic field on the resistivity of FeZrB glasses has also been studied. We found that a magnetic field of 4 T does not affect the thermal variation of the resistivity. A slight increase in the absolute values, of about 1%, was detected over the whole temperature range, but no significant changes in the T_{min}-values are observed. The increase in the value of $\rho(T)$ with the magnetic field, i.e. positive magnetoresistance, is related to a decrease of the electronic mean free path, and is characteristic of non-magnetic metals [37]. For the alloys for which measurements were made, this positive magnetoresistance overcomes the effect of the alignment of magnetic moments with the field, which tends to decrease the value of the magnetic contribution to the resistivity, i.e. negative magnetoresistance, for ferromagnetic materials. This behaviour agrees quite well with the previous studies of the magnetoresistance for $Fe_{100-x}Zr_x$ samples [38].

4. Discussion and conclusions

For the FeZrB alloys, we have observed that T_C decreases almost linearly when the Fe content increases from 86 to 91 at.%; see figure 8. At the same time, the Fe magnetic moment shows a similar behaviour. Measurements performed by Ryan *et al* [3] on pure $Fe_{100-x}Zr_x$ samples ($7 \leqslant x \leqslant 12$) show that T_C increases linearly with the Zr content. Data from Shirakawa *et al* [11], obtained on sputtered FeZr samples, show that T_C reaches a maximum value (286 K) at 20 at.% in Zr. In FeB glasses [25], the addition of boron up to 25–30 at.% enhances the value of the Curie temperature in a similar way to the addition of zirconium in the FeZr system. However, the iron magnetic moment remains almost constant; see figure 8. The relative effects of low amounts of boron and zirconium on the Curie temperature and magnetic moment seem to be similar. For high-Fe-content alloys, both B and Zr cause a linear increase. However, for lower percentages of Fe, the value of T_C levels off.

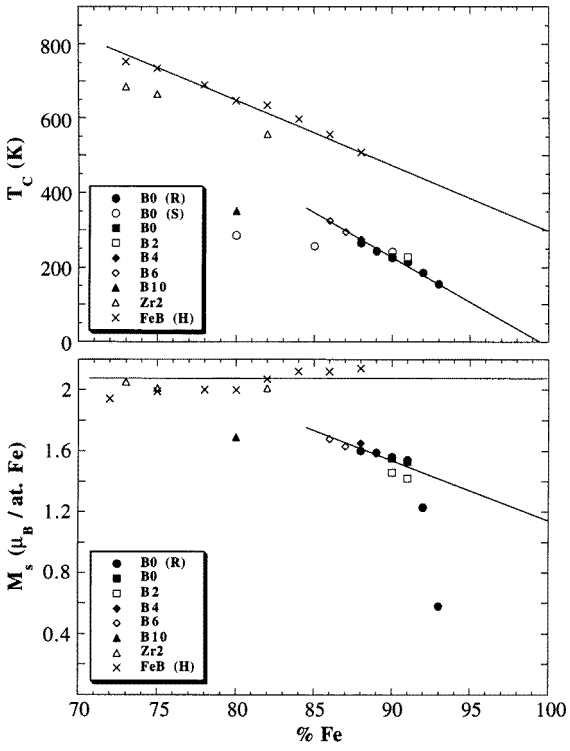

Figure 8. Curie temperatures (upper panel) and saturation magnetic moments (lower panel) for the different compositions studied. The data sets labelled (R), (H), and (S) have been taken from references [3], [25], and [11], respectively. The data set labelled (S) refers to sputtered samples. The Zr_2 data correspond in fact to samples of composition $Fe_{82}B_{16}Zr_2$, $Fe_{75}B_{23}Zr_2$, and $Fe_{73}B_{25}Zr_2$. Straight lines correspond to the extrapolation of the values to amorphous Fe.

To explain such behaviour, some authors have proposed a change of interaction between the Fe atoms, from antiferromagnetic to ferromagnetic, as the distance between them changes, at around a critical separation of about 2.54 Å [39]. Another alternative involves a moment instability as a function of the interatomic distance [40]. A change in the value of the magnetic moment or in the sign of the exchange interaction between Fe atoms as a function of the distance is unlikely to occur in our case, because the EXAFS determination of the Fe–Fe distances gives a constant value as a function of B content for low-boron-content alloys [16]. Moreover, the reduced-magnetization curves—figure 9—show only very slight changes when the amount of B or Zr varies, so the changes in T_C should arise directly from modifications of the exchange strength, but probably keeping the same ferromagnetic character.

At low boron concentration, the influences of B and Zr in the FeZrB alloys are similar. Moreover, a greater difference between the ZFC and FC curves is found for $Fe_{91}Zr_7B_2$ than for pure $Fe_{91}Zr_9$ glasses. In this part of the diagram, the extrapolation of T_C and μ_{Fe} to pure amorphous Fe gives a non-magnetic state ($T_C \approx 0$ K, $\mu_{Fe} \approx 1\ \mu_B$). On the other hand, small amounts of Zr greatly decrease the Curie temperature of the FeB alloys. Such alloys show an extrapolation to a magnetic amorphous Fe state with $T_C \approx 300$ K and $\mu_{Fe} \approx 2\ \mu_B$. This behaviour, clearly seen in figure 8, indicates completely different magnetic states for

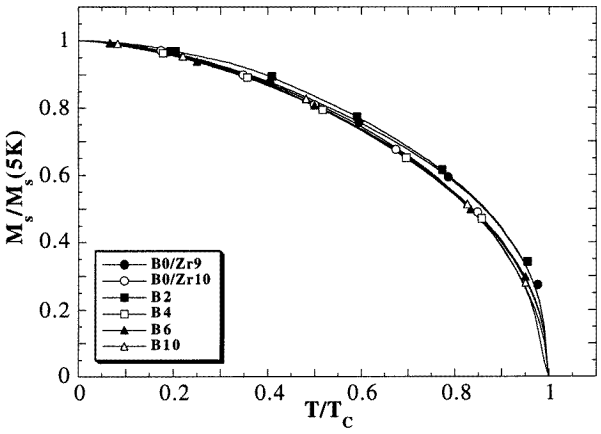

Figure 9. The reduced magnetization versus the reduced temperature for the samples B0, B2, B4, B6, and B10.

FeB and FeZr glasses. This probably arises from the different electronic transfers from Zr and B to Fe, giving rise to different band structures, which lead to changes in the DOS at the Fermi level $N(E_F)$, and the exchange splitting between the spin-up and spin-down sub-bands, which then causes changes in the itinerant character of their magnetism.

Among other techniques, specific heat measurements provide an estimate of $N(E_F)$, from the evaluation of the electronic contribution (γ_e) to the specific heat, as it is proportional to $N(E_F)$. Considering the limiting cases of pure FeZr ($Fe_{90}Zr_{10}$, $\gamma_e = 23.3$ mJ mol^{-1} K^{-2} [41]) and FeB ($Fe_{86}B_{14}$, $\gamma_e = 9.6$ mJ mol^{-1} K^{-2} [42]) alloys, it is straightforward to see a progressive decrease of the $N(E_F)$ when adding boron to the FeZr alloy. Moreover, previous experimental results for CoZr, CoZrAl [43], and CoB [44] glasses clearly show opposite trends for T_C and μ, on the one hand, and $N(E_F)$ on the other. In our case there is an increase of the T_C- and μ-values when B is added to the FeZr glasses, which agrees with the tendency of $N(E_F)$ expected from the values of γ_e for FeZr and FeB. However, one should be cautious when interpreting the high values of γ_e for FeZr alloys, because of the difficulties encountered in separating the electronic and magnetic contributions to the specific heat. The band calculations of the FeB [45] and FeZr [46] limiting cases could be used to anticipate the evolution of the band structures for the FeZrB intermediate alloys, which are not yet available. However, it is rather difficult to extract a detailed picture of $N(E_F)$, because of the special magnetic behaviour of FeZr alloys. Possible density fluctuations, inhomogeneities, spin clusters, and similar such considerations (important for DOS calculations) should be taken into account.

Another interesting feature of the magnetic behaviour, showing a continuous change as a function of the B content, is the magnetic inhomogeneity. This is deduced from the variations in the β- and a-parameters in the modified Arrott plots, and from the tails in the $P(B_{HF})$ obtained from Mössbauer spectroscopy. The inhomogeneity increases on approaching the pure FeZr side, i.e. when decreasing the B content. Such an inhomogeneity clearly causes the large coercivity observed in the alloys with re-entrant spin-glass-like behaviour. It turns out that a small percentage of boron atoms modifies the magnetic parameters drastically. However, for the sample B2, in which changes in the atomic structure related to the pure FeZr alloys are expected, the magnetic behaviour is still close to that of the $Fe_{91}Zr_9$ alloy, showing a broad $P(B_{HF})$ distribution, characteristic of the high magnetic

inhomogeneity of FeZr alloys [2, 3, 47].

The unusual resistivity behaviour of the FeZr-based alloys as a function of temperature, with a minimum at rather high temperatures close to T_C, greatly complicates the usual [34, 35, 48] data analysis. In the usual data analysis we try to identify and separate the diverse contributions to the electronic scattering according to Mathiessen's rule. We have attempted to follow this procedure for pure FeZr alloys [49, 50], showing the different contributions, but this is complicated by the number of independent contributions and their temperature dependences (for example, electron–phonon, magnon, and quantum corrections to the conductivity). An alternative approach, considering the tendencies and expected behaviour of the contributions rather than performing an exhaustive fitting evaluation, would be more convenient for these ternary alloys. This should allow us to extract and suggest the most plausible explanations for the very peculiar features of these variations.

From our data, the first fact to point out is that the existence of minima in the $\rho(T)$ curves has no direct relation to the spin-glass state, but seems to be of different origin. However, T_{min} and T_C follow the same trend for the FeZr-rich alloys, i.e. increasing with the boron percentage (see table 1). This is not the case for the alloys close to the limiting FeB alloys, for which the values of T_{min} are small (around 30 K), and T_C increases with the B content.

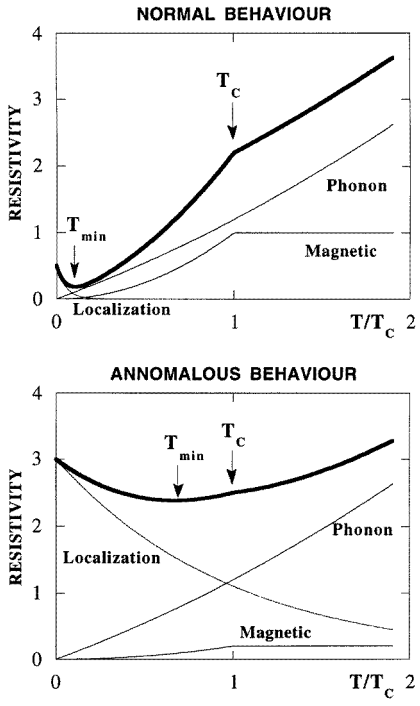

Figure 10. Theoretical simulations for the different contributions to the temperature dependence of the resistivity for amorphous alloys. The upper graph corresponds to 'normal behaviour', and the lower graph to 'anomalous behaviour'.

The comparison of the resistivities, depicted in figures 7 and 10, could provide some indications as to the origin of such a behaviour. Typically, in amorphous alloys, the larger contribution to the resistivity is the residual one, which is temperature independent.

In addition, we must consider temperature-dependent phonon [51], magnetic [34], and 'localization' scattering. A simplified scheme of the different temperature-dependent contributions to the resistivity is presented in figure 10 for FeZr and FeB alloys, in order to clarify the following discussion.

The main differences between the two cases are as follows.

(a) The magnetic contribution ρ_{mag} is much lower in the FeZr case, which must correspond to a lower T_C and weak ferromagnetic behaviour.

(b) The negative contribution at low temperatures, related to changes in the mobility of carriers, or 'localization', is small and decreases quickly with increasing temperature in the FeB case. For FeZr glasses, however, it must be much greater, and decrease slowly with increasing temperature, becoming negligible only well above T_C.

Figure 10 may assist in the explanation of the observed resistivity behaviour. For FeB amorphous alloys, T_C is clearly shown as a change in the $\rho(T)$ slope, while the small negative contribution, appearing at low temperatures, has been attributed to quantum localization effects [52]. For the FeZr and FeZrB samples with low B content, the magnetic contribution is much lower, and T_C is 'blurred' in the total $\rho(T)$ curve. Furthermore, experimentally, the minimum appears at a temperature close to T_C; this can be explained by the negative contribution becoming comparable to the phonon one at the ordering temperature. In this figure, figure 10, any possible contribution from the RSG state has been omitted (it should only be present on the FeZr side), because it can never be greater than the spin-disorder resistivity, which is constant above T_C, and is seen to be small.

The open question is, which is the scattering mechanism leading to this negative contribution? While in the FeB case, quantum localization effects have usually been invoked, in the FeZr case, the localization mechanism must be related in some way to the magnetic interactions. This strongly localizes the conduction electrons at low temperatures, but the effect decreases when the Curie temperature is approached. It would seem plausible that the ferromagnetic clusters or magnetic inhomogeneities, which, as discussed before, appear on the FeZr side, provide the centres of localization of electrons, while their absence in FeB would result in an absence of high-temperature minima in its $\rho(T)$ behaviour.

The above-suggested mechanism is reminiscent of a Kondo localization, which, when due to isolated magnetic impurities, disappears at low temperatures. In the present case, the large inhomogeneities should extend the localization to high temperatures. In fact, it has been suggested [5] that the magnetic clusters remain in a superparamagnetic state well above the Curie temperature of the matrix. This would explain the slow decrease of the above-mentioned electronic localization. Resistivity data obtained under pressure for FeZr alloys, [17] again reveal the correlation between T_C and T_{min}. A global increase of the density due to the pressure exerted can affect the clusters more deeply (because the matrix is close to the highest possible packing), thus reducing the number (or size) of these entities, and reducing the effect of the Kondo-like interaction.

From the results and discussion presented, it is clear that the magnetic behaviour of these alloys is mainly governed by the changes in the band structure, affecting the density of states at the Fermi level, rather than by modifications of the Fe–Fe distances. The addition of small amounts of B or Zr causes similar effects on T_C and μ_{Fe}, in spite of the very different sizes of these atoms. However, it is clear that the extrapolations to the pure Fe amorphous case from the FeZr or FeB side are very different (see figure 8), confirming that the band structures are very distinct, and lead to significantly different magnetic behaviours. On the other hand it would seem that if the magnetic inhomogeneities provide the basis for coercivity or re-entrant spin-glass behaviour, then they should also lie

at the origin of the resistivity behaviour found for the low-boron-content FeZrB alloys, in which an *enhanced electron localization* could be attributed to a Kondo-like mechanism, with clusters or inhomogeneities acting as localization centres.

Acknowledgments

The authors acknowledge the Spanish CICyT, through project MAT96-1023, and the Euskadi–Aquitaine agreement for financial support. The authors also acknowledge Professor O V Nielsen (Technical University of Denmark), and N Murillo (University of Pais Vasco) for help with the sample preparation, and Dr D Schmool for revision of the English in the manuscript.

References

[1] Hiroyoshi H and Fukamichi K 1982 *J. Appl. Phys.* **53** 2226
[2] Kaul S N, Siruguri V and Chandra G 1992 *Phys. Rev.* B **45** 12 343
[3] Ryan D H, Coey J M D, Batalla E, Altounian Z and Ström-Olsen J O 1987 *Phys. Rev.* B **35** 8630
[4] Fukamichi K, Goto T, Komatsu H and Wakabayashi H 1989 *Physics of Magnetic Materials* ed W Gorzkowski, H K Lachowicz and H Szymczak (Singapore: World Scientific) p 354
[5] Kiss L F, Kemény T, Vincze I and Gránásy L 1993 *J. Magn. Magn. Mater.* **135** 161
[6] Ren H and Ryan D H 1995 *Phys. Rev.* B **51** 15 885
[7] Kaul S N 1991 *J. Phys.: Condens. Matter* **3** 4027
[8] Kaptás D, Kemény T, Kiss L F, Balogh J, Gránásy L and Vincze I 1992 *Phys. Rev.* B **46** 6600
[9] Kiss L F, Kemény T, Vincze I and Gránásy L 1994 *J. Magn. Magn. Mater.* **135** 161
[10] Hegman N, Kiss L F and Kemény T 1994 *J. Phys.: Condens. Matter* **6** L427
[11] Shirakawa K, Kaneko T, Kanehira J, Ohnuma S, Fujimori H and Masumoto T 1982 *Proc. 4th Int. Conf. on Rapidly Quenched Metals (Sendai, 1981)* ed T Matsumoto and K Suzuki (Sendai: Japan Institute of Metals) p 1083
[12] Makino A, Suzuki K, Inoue A, Hirotsu Y and Masumoto T 1994 *J. Magn. Magn. Mater.* **133** 329
[13] Suzuki K, Makino A, Inoue A and Masumoto T 1991 *J. Appl. Phys.* **70** 6232
[14] Barandiarán J M, Gorria P, Gómez Sal J C, Fernández Barquín L and Kaul S N 1994 *IEEE Trans. Magn.* **30** 4776
[15] Barandiarán J M, Gorria P, Orúe I, Fernández-Gubieda M L, Plazaola F and Hernando A 1996 *Phys. Rev.* B **54** 3026
[16] Fernández-Gubieda M L, Gorria P, Barandiarán J M and Fernández Barquín L 1995 *Nucl. Instrum. Methods* B **97** 206
[17] Shirakawa K, Fukamichi K, Kaneko T and Masumoto T 1983 *Phys. Lett.* **97A** 213
[18] Shirakawa K, Fukamichi K, Kaneko T and Masumoto T 1986 *J. Phys. F: Met. Phys.* **14** 1491
[19] Pureur P, Schreiner W H, Kunzler J V, Ryan D H and Coey J M D 1988 *Solid State Commun.* **65** 163
[20] Babu P D, Kaul S N, Fernández Barquín L and Gómez Sal J C 1995 *J. Magn. Magn. Mater.* **140–144** 295
[21] Aharoni A 1984 *J. Appl. Phys.* **56** 3479
[22] Aharoni A 1985 *J. Appl. Phys.* **57** 648
[23] Wohlfarth E P 1977 *Physica* B **91** 305
[24] Chien C L, Musser D, Gyorgy E M, Sherwood R C, Chen H S, Luborsky F E and Walter J L 1979 *Phys. Rev.* B **20** 283
[25] Hasegawa R and Ray R 1978 *J. Appl. Phys.* **49** 4174
[26] Le Caër G and Dubois J M 1981 *Phys. Status Solidi* a **64** 275
[27] Brand R A, Lauer J and Herlach D M 1984 *J. Phys. F: Met. Phys.* **14** 555
[28] Billard L and Chamberod A 1975 *Solid State Commun.* **17** 113
[29] Hesse J, Müller J B and Weichmann B 1979 *J. Physique. Coll.* **40** C2 161
[30] Vincze I, Kaptás D, Kemény T, Kiss L F and Balogh J 1994 *Phys. Rev. Lett.* **73** 496
[31] Barandiarán J M, Gutiérrez J, Plazaola F and Zabala I 1987 *Proc. Symp. on Magnetic Properties of Amorphous Metals* ed A Hernando, V Madurga, M C Sánchez-Trujillo and M Vázquez (Amsterdam: North-Holland) p 142
[32] Banerjee N, Roy R, Majumdar A K and Hasegawa R 1981 *Phys. Rev.* B **24** 6801

[33] Mogro-Campero A and Walter J L 1979 *Phys. Rev.* B **20** 5030
[34] Kaul S N, Kettler W and Rosenberg M 1986 *Phys. Rev.* B **33** 4987
[35] Fernández Barquín L, Rodríguez Fernández J, Gómez Sal J C, Barandiarán J M and Vázquez M 1990 *J. Appl. Phys.* **68** 4610
[36] Fernández Barquín L, Rodríguez Fernández J, Gómez Sal J C, Gutiérrez J and Barandiarán J M 1991 *J. Magn. Magn. Mater.* **101** 52
[37] Pippard A B 1989 *Magnetoresistance in Materials* (Cambridge: Cambridge University Press)
[38] Ma M, Wang Z, Kunkel H P and Williams G 1992 *J. Phys.: Condens. Matter* **4** 1993
[39] Moruzzi V L, Marcus P M and Kübler J 1989 *Phys. Rev.* B **39** 6957
[40] Wassermann E F 1990 *Ferromagnetic Materials* vol 5, ed K H J Buschow and E P Wohlfarth (Amsterdam: North-Holland) p 305
[41] Obi Y, Wang L C, Motsay R, Onn D G and Nose M 1982 *J. Appl. Phys.* **53** 2304
[42] Matsuura M, Mizutani U and Tazawa Y 1981 *J. Phys. F: Met. Phys.* **11** 1393
[43] Kanemaki S, Takehira O, Goto T and Mizutani U 1992 *J. Phys.: Condens. Matter* **4** 2217
[44] Mizutani U, Hasegawa M, Fukamichi K, Hattori Y, Yamada Y, Tanaka H and Takayama S 1993 *Phys. Rev.* B **47** 2678
[45] Bratkovsky A M and Smirnov A V 1993 *Phys. Rev.* B **48** 9606
[46] Turek I, Becker C and Hafner J 1992 *J. Phys.: Condens. Matter* **4** 7257
[47] Ghafari M, Gonser U, Wagner H G and Naka M 1982 *Nucl. Instrum. Methods* **199** 197
[48] Das A and Majumdar A K 1991 *Phys. Rev.* B **43** 6042
[49] Fernández Barquín L, Gómez Sal J C, Babu P D and Kaul S N 1994 *J. Magn. Magn. Mater.* **133** 82
[50] Babu P D, Kaul S N, L. Fernández Barquín and Gómez Sal J C 1995 *J. Magn. Magn. Mater.* **140–144** 295
[51] Nagel S R 1977 *Phys. Rev.* B **16** 1694
[52] Howson M A and Gallagher B L 1988 *Phys. Rep.* **170** 265